[CANCER RESEARCH 63, 2681–2687, May 15, 2003]

3′-[^{18}F]Fluoro-3′-Deoxythymidine ([^{18}F]-FLT) as Positron Emission Tomography Tracer for Imaging Proliferation in a Murine B-Cell Lymphoma Model and in the Human Disease

Martin Wagner,[2] Ulrike Seitz,[1,2] Andreas Buck, Bernd Neumaier, Stefan Schultheiß, Markus Bangerter, Martin Bommer, Frank Leithäuser, Edgar Wawra, Gerd Munzert, and Sven N. Reske

Departments of Nuclear Medicine [U. S., A. B., B. N., S. S., S. N. R], Internal Medicine I [M. W., M. Ba.], Internal Medicine III [M. Bo., G. M.], Pathology [F. L.], University of Ulm, 89081 Ulm, Germany and Vienna Biocenter, Institute of Molecular Biology, University of Vienna, A-1030 Vienna [E. W.]

ABSTRACT

Here we describe the evaluation of 3′-[^{18}F]fluoro-3′-deoxythymidine {[^{18}F]-FLT} as a tracer for positron emission tomography (PET) in a murine model of B-cell lymphoma and in human malignant lymphoma. The human B-cell line DoHH2 expressed high levels of active thymidine kinase 1 (TK-1) as the key enzyme of [^{18}F]-FLT metabolism. Immunostaining confirmed high levels of TK-1 in DoHH2 derived xenograft tumors in SCID/SCID mice. *In vitro* studies demonstrated a time-dependent uptake of [^{18}F]-FLT, an efficient phosphorylation to the respective monophosphate and the incorporation of [^{18}F]-FLT into the perchloric acid insoluble fraction in DoHH2 cells, indicating the incorporation of this tracer into the DNA. After incubation with [^{18}F]FLT for 240 min, 12.5% ± 1.0% of radioactivity applied to the medium was intracellularly trapped in DoHH2 cells. Specific accumulation of [^{18}F]-FLT in the malignant cell clone was confirmed in biodistribution studies in SCID/SCID mice bearing DoHH2-derived tumors. The percentage of injected dose of [^{18}F]-FLT per gram of tumor tissue correlated with the tumor-proliferation index as evaluated in BrdUrd-labeling experiments. In a pilot study of 11 patients with both indolent and aggressive lymphoma, [^{18}F]-FLT was suitable and comparable to [^{18}F]-FDG in the ability to detect malignant lesions by PET scan. Furthermore, we found a close correlation ($r = 0.95$, $P < 0.005$) of the [^{18}F]-FLT standardized uptake values with the Ki67-labeling index of tissue biopsies ($n = 10$) in these patients. These results suggest that [^{18}F]-FLT represents a novel tracer for PET that enables imaging of proliferation in human lymphoma *in vivo*.

INTRODUCTION

PET[3] represents an analytical technology that uses compounds labeled with positron emitting radioisotopes as molecular probes to image and measure biochemical processes *in vivo*. Currently, FDG is the most widely used PET tracer in clinical oncology. Viable tumor cells display an increased intracellular influx of the glucose analogue FDG via overexpression of glucose transporters and a higher rate of intracellular phosphorylation through the hexokinase pathway which results in an intracellular trapping of FDG-6-phosphate in cancer cells (1–3).

The strength of FDG-PET in diagnosis and staging of malignant lymphoma has been evaluated and compared with conventional staging methods as CT, ultrasonography, or magnetic resonance tomography in several studies (4–6). FDG-PET has been shown to be more sensitive in the detection of nodal (6), extranodal (7), and bone marrow (5, 8) involvement as compared with CT scans. The lack of FDG uptake in residual masses after completion of therapy is associated with a high probability of long term disease free survival (9). However, the diagnostic accuracy of FDG-PET in the evaluation of indolent malignant lymphoma remains under discussion (10). In this regard, a quantitative estimate of the proliferative activity of a tumor obtained through noninvasive imaging would aid in selecting sides for biopsy, optimal treatments for patients and could provide a more accurate assessment of the response to therapy.

Pyrimidine nucleosides and several of their analogues are phosphorylated to the respective monophosphate (MP) by thymidine kinase 1 (TK-1) and are incorporated into DNA, partly acting as chain terminators. More than 40 years after its invention, [^{3}H]thymidine remains the gold standard to measure cell proliferation *in vivo*. Positron-emitting radionuclides enable *in vivo* imaging of deregulated proliferation with PET as one of the key features of malignant disease. [^{11}C]-labeled thymidine has been proposed as a radio tracer for imaging tumor proliferation by several groups (11, 12). Furthermore, we have recently shown that uptake of [^{18}F]fluorodeoxyuridine *in vivo* correlates with the proliferation in a murine pancreatic cancer model (13). However, the metabolic instability of both tracers represents the major drawback for routine clinical applications. As a more recent development, 3′-[^{18}F]fluoro-3′-deoxythymidine {[^{18}F]FLT} was used with highly promising results (14–16). 3′-fluoro-3′-thymidine (FLT) has been identified as a nucleoside analogue with antiretrovirus activity (17). FLT permeates the cell membrane by a carrier-mediated mechanism, as well as by facilitated diffusion (18, 19), and is phosphorylated to 3′-fluorothymidine MP (FLT-MP) through the S-phase specific enzyme TK-1 (see Ref. 17; for review, see 20). This phosphorylation results in intracellular trapping of FLT-MP. High levels of TK1 activity have been reported for rapidly growing cells and tumor tissues (21–23).

Here we report high levels of active TK-1 in DoHH2 cells (24, 25) and in DoHH2 cells derived xenograft tumors in SCID/SCID mice as a murine model of human B-cell lymphoma (26). In this model and in a pilot study of human malignant lymphoma, we have evaluated [^{18}F]FLT as a PET tracer for imaging proliferation *in vivo*.

MATERIALS AND METHODS

Cell Culture and SCID/SCID Lymphoma Model. Human non-Hodgkin's B-cell lymphoma cell line DoHH2 (24, 25) and EBV-transformed human lymphocytes were maintained in RPMI 1640 medium supplemented with 10% FCS (Life Technologies, Inc., Berlin, Germany). The fibroblast cell line HT1080 (ATTC, Washington, D.C.) was grown to confluence to induce growth arrest through contact inhibition as described. According to Cotter *et al.* (26), tumor cells (10^6 cells in 100 μl) were administered by s.c. route to CB-17 SCID/SCID mice weighing 30–35 g. At 3–4 weeks posttransplantation, the mice developed lymphomas weighing ~2.0 g.

Quantitative RNA Analysis. The ABI Prism 7700 Sequence Detection System (Perkin-Elmer Applied Biosystems, Foster City, CA) was used for real-time monitoring of PCR amplification of the c-DNA, and the target c-DNA was quantified using the delta-delta-CT method as described (27). The

Received 8/14/02; accepted 3/13/03.

The costs of publication of this article were defrayed in part by the payment of page charges. This article must therefore be hereby marked *advertisement* in accordance with 18 U.S.C. Section 1734 solely to indicate this fact.

[1] To whom requests for reprints should be addressed, at Department of Nuclear Medicine, University of Ulm, Robert-Koch-Str. 8, D-89081 Ulm, Germany. Phone: 49-731-500-33864; Fax: 49-731-500-24979; E-mail: ulrike.seitz@medizin.uni-ulm.de.

[2] Both authors contributed equally to this work.

[3] The abbreviations used are: PET, Positron emission tomography; FDG, 2-deoxy-2-[^{18}F]fluoro-D-glucose; CT, computed tomography; MRI, magnetic resonance tomography; TK, thymidine kinase; [^{18}F]FLT, 3′-[^{18}F]fluoro-3′-deoxythymidine; FLT, 3′-fluoro-3′-thymidine; MP, monophosphate; BrdUrd, bromodeoxyuridine; FP, forward primer; RP, reverse primer; high-performance liquid chromatography; ID, injected dose; SUV, standardized uptake value.

following forward (FP) and reverse (RP) primers were used: TK-1-FP (300 nM), 5′-GGG GCAGATCCAGGTGATTC-3′; TK-1-RP (150 nM), 5′-GCATACTTGATCACCAG-GCACTT-3′; cyclophilin-FP (300 nM), 5′-ATG-GTCAACCCCACCGTGT-3′; and cyclophilin-RP (300 nM), 5′-TCTGCT-GTCTTTGGGACCTTGTC-3′. The specificity of the reaction was confirmed by electrophoresis on a 4% low-melting agarose gel showing a single band with the predicted size for each of the primer pairs mentioned.

Measurement of TK-1 Activity by Flow Cytometry. TK-1 activity was measured as described previously (27). Briefly, cells were exposed to 1.5 μmol/l fluorescent thymidine analogue AudR/DANS for 1 h at 37°C in serum-free DMA medium. The cells were washed and centrifuged, and the pellet was resuspended in cold PBS. For DNA staining 25 μmol/l ethidium bromide (Serva, Heidelberg, Germany) was used. Fluorescence from TK-1 activity and DNA was simultaneously measured with a Partec PAS-II flow cytometer using a mercury lamp to excite AUdR/DANS at 380–420 nm and measuring emission at 450–500 nm. Fibroblasts from TK-1-deficient mice served as a negative control, whereas EBV-transformed lymphocytes were used as a positive control as described (27).

[^{18}F]FLT Synthesis. [^{18}F]FLT was synthesized by nucleophilic substitution using trityl-protected anhydrothymidine as described with minor modifications (27–29). [^{18}F]fluoride was produced via the ^{18}O(p,n)^{18}F nuclear reaction at the Cyclone 18/9 IBA cyclotron.

Cell Uptake Studies and Incorporation of [^{18}F]FLT into DNA. For cell-uptake studies, cells were cultured for 24 h in 6-well plates and were incubated with either 0.07 MBq/ml [^{18}F]FDG or [^{18}F]FLT at 37°C for 15, 30, 45, 60, 120, and 240 min. At the end of each incubation period, radioactivity in the medium was measured. The wells were harvested, washed twice with ice-cold phosphate buffered saline (PBS), and the cell-associated radioactivity was determined. The cellular pellet was lysed in 200 μl (RBS, 5% NP40, RNase A 200 μg/ml) for 15 min at 37°C followed by 15 min incubation at 37°C in the presence of proteinase K (1 mg/ml). Quantitative DNA recovery was performed through perchloric acid precipitation as described (27, 30). The radioactivity associated with the acid-soluble and the acid-insoluble fractions was counted and corrected for decay and the number of cells. The radioactivity in the acid-insoluble fraction represents the phosphorylated metabolite incorporated in the DNA. Quadruplicate samples were performed at each time point for all uptake studies. To evaluate the protein contamination in the acid insoluble fraction, the protein content was measured in the initial cell lysate as well as in the acid insoluble pellet (Bradford reagent). Quantitative DNA recovery was confirmed through DNA measurement via DNA precipitation with the diphenylamine reagent as described (27, 30). The data are displayed as mean and SD of at least four experiments.

High-Performance Liquid Chromatography Analysis of [^{18}F]FLT Metabolites in Cells. The acid-soluble fraction (incubation time 1 h, 2 million cells, applied radioactivity 1 MBq/ml) was analyzed by high-performance liquid chromatography (HPLC) as described (27). The FLT-MP standard was established as described (27).

Murine Biodistribution Studies. [^{18}F]-FLT was injected i.v. into a tail vein at a mean dose of 0.1 MBq. Six to seven mice were sacrificed 15 to 90 min after injection. Blood samples were obtained and the tumor and organs weighed, assayed for radioactivity, and corrected for decay. Data were expressed as mean percentage of ID/g of tissue (%ID/g) and SD of several experiments.

Histological Examination and Immunostaining. Tumors and tissues from experimental animals were fixed in 4% neutral buffered formalin, processed, embedded in paraffin wax, sectioned, and stained with hemotoxylin and eosin. For *in vivo* BrdUrd-labeling animals were injected with 1 ml/100 g BrdUrd solution (Amersham Pharmacia Biotech, United Kingdom) 3 h before sacrifice. Immunostaining for BrdUrd incorporation was performed on paraffin sections with a monoclonal anti-BrdUrd antibody following the manufacturers recommendations (Boehringer Mannheim, Germany). Immunoflurorescence staining was performed as reported previously (13, 27).

Assessment of the Proliferation Index. For the proliferation index based on BrdUrd staining, six randomly selected sections were analyzed for the number of positive nuclei in relation to the total number of nuclei using Image-Pro Express (Media Cybernetic L. P., Silver Spring, MD). On average, 695 ± 95 nuclei were analyzed for each section. The proliferation index and the %ID/g were analyzed for correlation with Pearsons Multiple Regression using GraphPad Prism (GraphPad Software Inc., San Diego, CA).

PET Imaging of Patients with [^{18}F]FLT. Eleven patients with histologically proven malignant lymphoma participated in the study. Static whole body scans were performed with an ECAT Exact full-ring scanner (Siemens, Munich, Germany) 60 min postinjection of [^{18}F]FLT (mean dose, 280 MBq) or [^{18}F]FDG (mean dose, 570 Mbq) followed by iterative reconstruction. Images were interpreted by two experienced physicians unaware of the patients condition. SUVs of positive findings were calculated. For blood clearance and evaluation of metabolites with HPLC plasma and urine samples were obtained from selected patients (n = 4) after FLT injection. On the basis of findings of [^{18}F]FLT PET (31) sides of tissue biopsy (n = 9) and fine-needle aspiration cytology (n = 1) were selected. The proliferation rate was evaluated as percentage of Ki67/MIB-1 positive cells after immunohistochemical staining of tissue sections as outlined above (n = 7) or with cytology and FACS-analysis of Ki67/MIB-1 stained cells (n = 1). For FACS analysis the aspiration was suspended in 10 ml of PBS, counted (ADVIA, Bayer Diagnostics), incubated with a FIX+PERM Permeabilization-Kit (Dianova, Hamburg, Germany), followed by ice cold methanol, and centrifuged for 5min at 300*g*. After washing the pellet, cells were labeled with FITC-labeled MIB-1 antibody 606F (Dianova, Hamburg, Germany), counterstained with PE-labeled CD79a antibody (DAKO, Denmark) and analyzed with flow cytometry (Becton Dickinson, San Jose, CA). Proliferation index was assessed as the percentage of cells stained with MIB-1 and positive for CD79a. Informed consent was obtained of all patients participating in the study. The ethics committee of the University of Ulm approved the study protocol.

RESULTS

Evaluation of TK-1 Expression in the DoHH2 Cell Line and in Xenografts. Taqman analysis indicated a 2-fold up-regulation of mTK1 mRNA in the established B-cell lymphoma cell line (DoHH2) compared with EBV-transformed human B-lymphocytes (data not shown). The expression of enzymatic active TK-1 in the DoHH2 cells was further confirmed by flow cytometry. EBV-transformed lymphocytes were used as internal positive controls for the assay becasue recent data demonstrated a >100-fold increase of TK-1 activity in these cells as compared with nonstimulated lymphocytes (32). As demonstrated in Fig. 1*A*, TK-1 activity in DoHH2 cells was 2.9-fold higher as compared with the EBV-transformed lymphocytes.

Injection of DoHH2 cells into immunodeficient SCID/SCID mice resulted in lymphoma development as described (26). These xenografts expressed high levels of TK-1. Shown in Fig. 1*B* is cytoplasmic staining in the tumor cells, whereas noninfiltrated lymph nodes showed only minor staining (data not shown). Further evaluation of TK-1 expression in several murine tissues including liver, spleen, kidney, small intestine, heart, skeleton muscle, and lung demonstrated TK-1 expression in the spleen (Fig. 1*C*), but not in the other tissues such as *e.g.*, the liver (Fig. 1*D*).

Synthesis of FLT. [^{18}F]FLT was synthesized as described (28, 29). The radiochemical purity of [^{18}F]FLT in isotonic sodium chloride solution was >98% as analyzed with analytical HPLC. The mean activity concentration was 2 GBq/6 ml. The overall effective radiochemical yield was 5–10%, *i.e.*, 25 GBq [^{18}F]Fluoride resulted in 2000 MBq of [^{18}F]FLT (data not shown).

***In vitro* Uptake of [^{18}F]FLT.** Displayed in Fig. 2*A* is the uptake kinetic of [^{18}F]FLT in DoHH2 and growth arrested HT1080 cells as compared with the uptake of [^{18}F]FDG. The uptake of [^{18}F]FLT into DoHH2 cells increased from 1.8% ± 0.8% of the applied radioactivity in the medium after 15 min to 12.5% ± 1.0% after 240 min of incubation (Fig. 2*A*, *open triangles*). In HT1080 cells, cell-bound radioactivity reached only 1.7% ± 0.08% of the applied radioactivity after 240 min of incubation with [^{18}F]FLT (Fig. 2*A*, *open circles*). Furthermore, the cellular uptake of [^{18}F]FDG was only 2.1% ± 0.8% in DoHH2 cells (Fig. 2*A*, *closed triangles*), whereas HT1080 cells took up 3.9% ± 0.4% of [^{18}F]FDG after 240 min (Fig. 2*A*, *closed circles*).

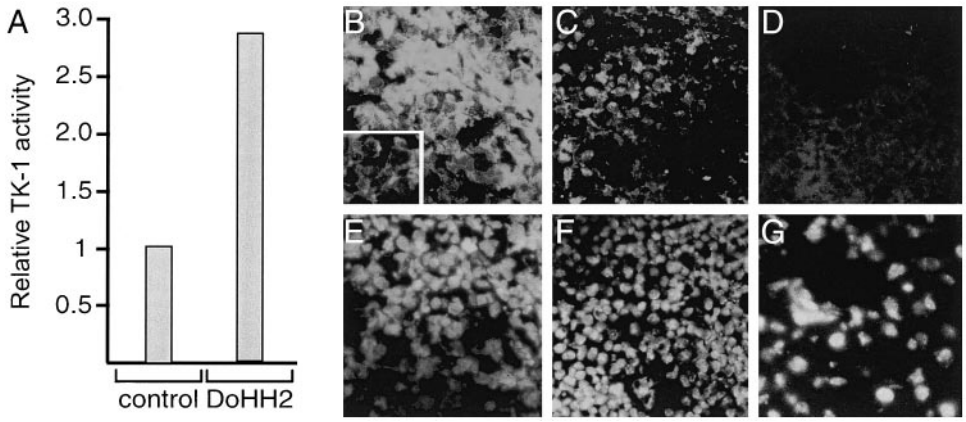

Fig. 1. *A*, Flow cytometric measurement of TK-1 activity in DoHH2 cell compared with TK-1 activity in EBV-transformed lymphocytes as a positive control. Values are expressed as multiples of TK-1 activity in the positive control. *B–G*, immunofluorescence staining demonstrated cytoplasmatic TK-1 expression in xenograft tumor cells (*B*) and to a lesser extent in the spleen (*C*). No staining was found in the liver (*D*). *E–G* depict the corresponding nuclear counter staining. Original magnification was ×50 in *B–G* and ×160 (*inset* in *B*).

Depicted in Fig. 2*B* are typical HPLC chromatograms of the *in vitro* phosphorylated FLT (FLT-MP, UV detection) and of FLT-MP together with FLT (FLT-MP and FLT, UV detection). The *lower panel* displays HPLC analysis of the cellular lysate of DoHH2 cells after an incubation time of 60 min with [^{18}F]FLT. The appearance of the additional peak on γ-detection at a retention time of 10 min indicates the efficient phosphorylation of [^{18}F]FLT (retention time 19.5 min) to the respective MP.

Furthermore, we evaluated the [^{18}F]FLT derived radioactivity associated with the perchloric acid insoluble fraction in DoHH2 cells. Following the applied protocol (27, 30), we confirmed quantitative DNA recovery and an average protein recovery of 1.1% ± 0.1% with

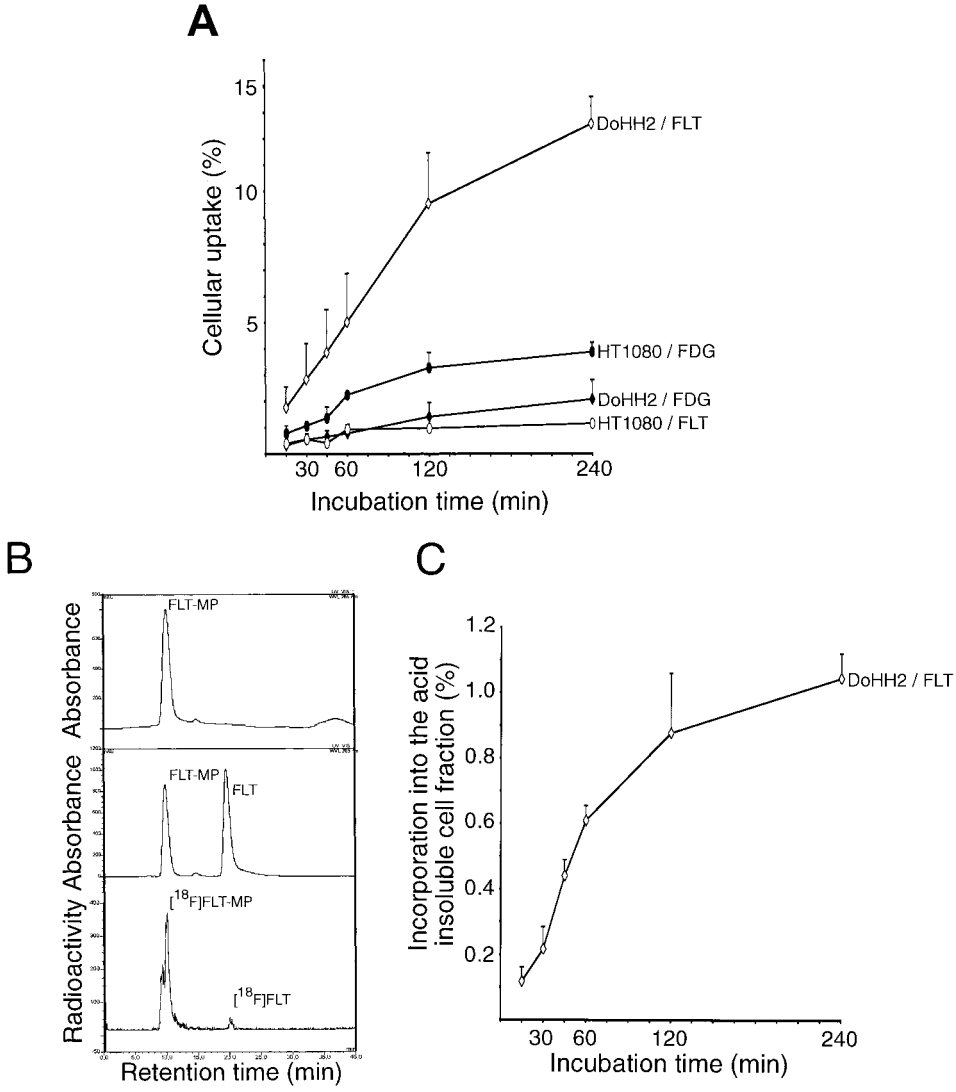

Fig. 2. *A*, cellular uptake of [^{18}F]FLT (◇) and [^{18}F]FDG (♦) in DoHH2 cells was compared with growth arrested HT1080 cells (○ and ●, respectively). Data are expressed as the percentage of uptake of the [^{18}F]FLT- or [^{18}F]FDG-derived radioactivity applied to the medium. *Error bars* depict SD (n = 4). *B*, HPLC analysis of [^{18}F]FLT in DoHH2 cells after an incubation time of 60 min. The *upper panel* depicts the *in vitro* phosphorylated FLT-MP standard (FLT-MP) and the *middle panel* displays analysis of the standard together with FLT upon UV detection (absorbance, 265 nm). HPLC analysis of cellular lysate of DoHH2 cells (*lower panel*) demonstrate phosphorylated [^{18}F]FLT with a retention time 10 min compared with the paternal compound (retention time, 20 min). *C*, incorporation of [^{18}F]FLT into the acid insoluble fraction of DoHH2 cells (△). The radioactivity detected in the perchloric acid insoluble fraction was expressed as a percentage of the radioactivity applied to the medium. *Error bars* depict SD (n = 4).

DNA and protein measurement, respectively (data not shown). [^{18}F]FLT-derived radioactivity associated time dependent with the perchloric acid insoluble fraction of $DoHH_2$ cells (Fig. 2*C*), but not with the perchloric acid insoluble fraction of HT1080 cells (data not shown). After 240 min, 1.05% ± 0.08% of the radioactivity applied to the medium was trapped in the acid insoluble fraction in DoHH2 cells (Fig. 2*C*). In contrast, [^{18}F]FDG was not incorporated into the perchloric acid insoluble fraction (data not shown).

Biodistribution of [^{18}F]FLT in the DoHH2/SCID Mouse Lymphoma Model. Tissue distribution of [^{18}F]FLT in lymphoma-bearing SCID-mice was assessed by tissue sampling and by gamma spectroscopy at 15 to 90 min after injection of 0.1MBq [^{18}F]FLT (Fig. 3*A*).

Tumor tissue displayed a time dependent accumulation of [^{18}F]FLT reaching 7.39 ± 5.49% of the %ID/g after 60 min and only slightly decreasing after 90 min (Fig. 3*A*). In sharp contrast, the distribution of [^{18}F]FLT in the majority of nondiseased tissues displayed a washout kinetic with the highest levels measured after 15 min and a steady decrease thereafter. No measurable uptake was evident in the brain. However, [^{18}F]FLT accumulated in the spleen with a kinetic comparable to the tumor tissue. The %ID/g of [^{18}F]FLT in the spleen was ~3-fold higher as in tumor (Fig. 3*A*).

The %ID/g of [^{18}F]FLT correlated with the proliferation index as determined with *in vivo* BrdUrd-labeling experiments and morphometric analysis of tumor samples (Fig. 3*B*). Multiple regression analysis resulted in a regression coefficient $r = 0.63$ ($P < 0.05$). The comparison of the proliferation with the [^{18}F]FLT uptake to the small intestine failed to prove any correlation. The [^{18}F]FLT uptake and the proliferation in the spleen displayed only minor correlation (data not shown).

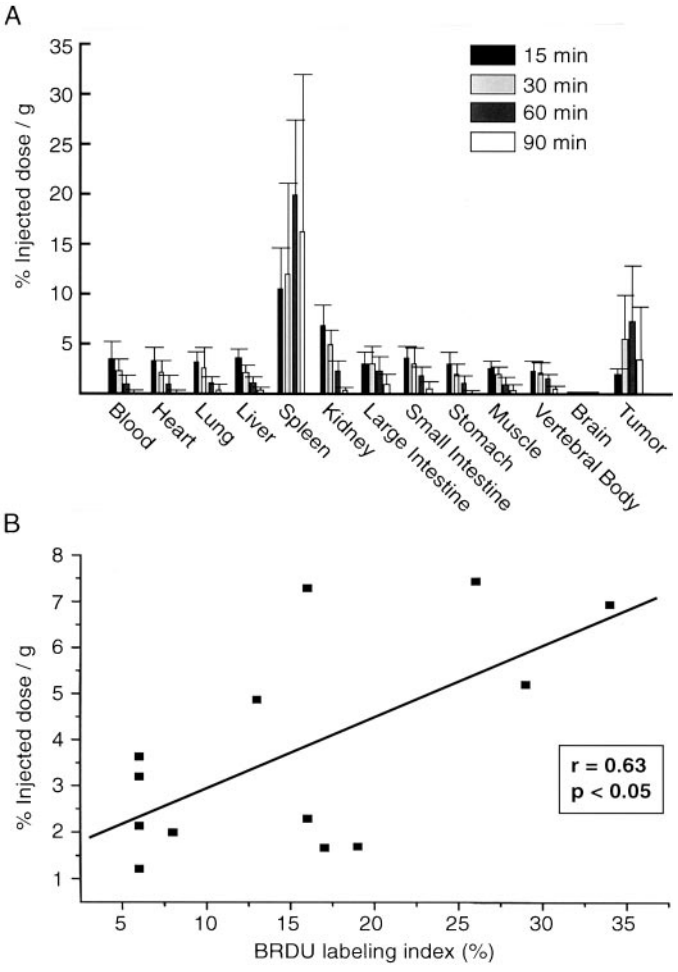

Fig. 3. *A*, biodistribution of [^{18}F]FLT in CB-17 SCID/SCID mice after single i.v. injection of 0.1 MBq over a period of 90 min. Results were expressed as %ID/g of tissue. *Error bars* depict SD ($n = 4$ to 8). *B*, multiple regression analysis of the %ID/g of tumor tissue and the BrdUrd-labeling index. Each *point* represents data from tumor tissue of an individual mouse.

Imaging Human Lymphoma with [^{18}F]FLT. *In vivo* stability of [^{18}F]FLT in the serum of selected patients ($n = 4$) was confirmed with HPLC analysis. Thirty minutes after [^{18}F]FLT injection no major radioactive metabolites were evident during γ-detection (Fig. 4*A*, *middle panel*). The blood-clearance curve of [^{18}F]FLT showed a biexponential elimination pattern 43% ± 6% being cleared with a half-time of 5.6 ± 2.0 min, followed by a slow component 57% ± 6% with a half-time of 95 ± 17 min, with an initial distribution volume of 29 liters for a 70-kg patient (data not shown). HPLC analysis of the urine detected 35% of the activity running with a retention time of 20 min indicative for the parent compound (Fig. 4*A*, *lower panel*). In addition, the urinary HPLC profile displayed an additional peak with a slightly shorter retention time as FLT-MP (Fig. 4*A*) suggestive of the excretion of the 5′-glucuronide of [^{18}F]FLT.

In a pilot study, we compared the ability of [^{18}F]FLT with [^{18}F]FDG to detect malignant lesions in patients with histologically proven lymphoma. Informed, written consent was obtained from the patients ($n = 11$) participating in the study. Table 1 summarizes the patients characteristics. PET scans with [^{18}F]FLT and [^{18}F]FDG ($n = 9$) were performed on consecutive days with the same PET scanner and the number of lesions detected with either scan being compared. These results indicate that both tracers detected comparable number of lesions (Table 1). Depicted in Figs. 4 *B* and *C* are PET findings in a 70-year-old patient (patient no. 6) with follicular center lymphoma in transformation (grade 3). Whole body distribution of [^{18}F]FLT in all patients showed intense accumulation of the tracer in the hematopoietic bone marrow and the liver. Urinary excretion was demonstrated by the accumulation of the tracer and putative metabolites in the kidneys and the bladder (Fig. 4*B* and *C*). Furthermore, [^{18}F]-FLT detected two occipital lesions in this patient with maximum SUVs of 11.0 (lesion 1) and 8.0 (lesion 2), respectively (Fig. 4*C*). This related to 20.3% Ki67 positive cells in lesion 1, whereas only 9.0% of cells were Ki67 positive after FACS analysis in lesion 2.

To analyze the relation of proliferation and SUV in more detail, we evaluated the proliferation index of selected tumor sides from 8 additional patients with Ki67 staining of tissue biopsies ($n = 10$) and compared this with the SUV obtained for each lesion. We found a close correlation of the proliferation index with the SUV in 8 of 9 patients in our group (Fig. 4*D*). Multiple regression analysis (for the patients nos. 1, 2, 5, 6, 7, 8, and 9) resulted in a regression coefficient of 0.94 ($P < 0.005$). However, in one patient with an anaplastic large cell lymphoma (patient no. 11), the SUV was only 6, whereas 90% of cells were positive for Ki67 (Fig. 4*D*, data point marked with an *asterisk*). Histological examination of this lymphoma showed marked fibrosis accounting for >30% of the tissue. Thus, the low cellularity and the desmoplastic reaction of this tumor explained the low uptake of [^{18}F]FLT.

DISCUSSION

Molecular imaging with PET visualizes alterations of biochemical pathways *in vivo*. In this regard, PET using the tracer FDG measures the high glucose metabolism and increased rate of glucose consumption in cancers that are associated with changes in the level of glycolytic enzymes and the overexpression of the glucose transporter 1 and 3 (2, 3). However, high FDG accumulation within experimental tumors has been shown to be associated with morphological changes of hypoxia ischemia, impending necrosis, and inflammatory response

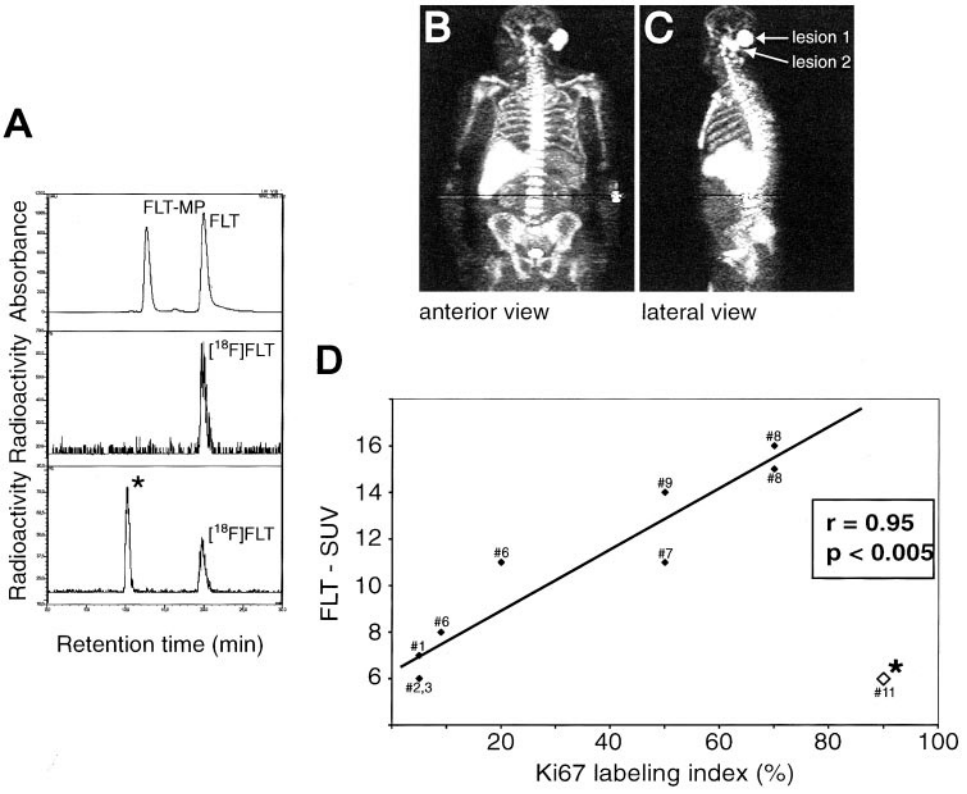

Fig. 4. *A*, HPLC analysis of [^{18}F]FLT metabolites in serum (30 min after injection; *middle panel*) and the urine (*lower panel*) of a representative patient. The *upper panel* depicts the *in vitro* phosphorylated FLT-MP together with FLT after UV detection (absorbance 265 nm). *B* and *C*, PET imaging of a patient with cytologically proven follicular lymphoma in transformation detected two occipital lesions with different SUVs. Pronounced uptake of [^{18}F]FLT was seen in the liver and the red bone marrow. *D*, multiple regression analysis of [^{18}F]FLT maximum SUV 1 h after injection and the Ki67-labeling index of selected biopsies (n = 10). Each *point* is marked with the patients identification no. from Table 1. Patient no. 11 was not included in the regression analysis and is marked with an *asterisk*.

(33, 34). In this respect, inflammatory lesions show an increased uptake of FDG and are the most frequent cause of false-positive results (33–35). In contrast, the uptake of pyrimidine nucleosides and analogues such as [^{18}F]-FLT relates to the proliferative activity in the tissue as one of the key features of malignant disease. Recent advances in the labeling of FLT (28, 29), as used in this study, enable the synthesis of [^{18}F]-FLT in high radiochemical yield and with high radiochemical purity suitable for *in vitro* evaluation and PET imaging studies.

TK-1 represents the rate-limiting enzyme for the anabolism of several pyrimidine analogues, such as FLT through the salvage DNA synthesis pathway, and displays a complex S-phase regulated expression that is realized not only at the transcriptional level, but also the posttranscriptional level and posttranslational mechanisms (21, 36). The salvage pathway of DNA synthesis includes deoxycytidine kinase, TK-1, TK-2, and deoxyguanosine kinase; however, only TK-1 accepts FLT as a substrate (37). Here we show that TK-1 m-RNA is increased in DoHH2 cells. The DoHH2 cells originated from a patient with immunoblastic lymphoma (24), and DoHH2 derived xenograft tumors were used as a murine model of human malignant lymphoma in this study (26). Because a recent study reported a discrepancy of human TK-1 mRNA and enzymatic activity in patients with chronic lymphatic leukemia (38), we further confirmed active TK-1 in a fluorocytometric assay. Furthermore, high levels of TK-1 are evident in DoHH2-derived xenograft tumors in SCID/SCID mice as reported for rapidly growing tissues (23). These data indicated that DoHH2 cells and derived xenograft tumors are suitable for the *in vitro* and *in vivo* evaluation of [^{18}F]-FLT as PET tracer.

In vitro, DoHH2 displayed progressive intracellular accumulation of [^{18}F]-FLT. Interestingly, [^{18}F]-FLT uptake was substantially higher than FDG uptake in DoHH2 cells, whereas growth arrested HT1080 cells displayed an inverse relation. Furthermore, [^{18}F]-FLT is effi-

Table 1 *Characteristics of patients with histologically proven lymphoma*

Patient no.	Sex	Age (yr)	Histological subtype	Lesions detected both with FLT and FDG (n)	Lesions detected only with FLT (n)	Lesions detected only with FDG (n)	Localization of biopsy	Ki67-positive cells (%)	FLT (maximum SUV)
1	Male	70	Follicular	5	2	0	Cervical	5	7
2	Female	54	Immunocytoma	ND[a]	3	ND	Cervical	5	6
3	Female	69	Mantle cell	11	0	0	ND	ND	ND
4	Female	65	Follicular	1	0	2	ND	ND	ND
5	Male	38	Follicular	10	1	2	Inguinal	5	6
6	Male	70	Follicular/in transformation	2	0	0	Skull*	20	11
							Skull*	9	8
7	Male	55	Follicular/in transformation	ND	3	ND	Soft tissue	50	11
8	Male	39	Large cell diffuse	ND	2	ND	Abd. bulk (1)	70	16
							Abd. bulk (2)	70	15
9	Male	39	Large cell diffuse	2	2	1	Cervical	50	14
10	Male	63	Large cell diffuse	13	0	0	ND	ND	ND
11	Male	43	Large cell anaplastic	3	0	0	Lung	90	6

[a] ND, not determined; Abd., abdominal.
* denotes lesions and depicted in Figure 4C.

ciently phosphorylated and incorporated into the perchloric acid insoluble cell fraction of DoHH2 cells *in vitro*. This intracellular trapping of [^{18}F]-FLT after phosphorylation represents a key determinate for using [^{18}F]-FLT as a proliferation marker *in vivo* (16, 39). Furthermore, these data suggest that [^{18}F]-FLT is incorporated into the DNA under the applied conditions. This is supported through previous reports that evaluated FLT as an antiviral drug with activity against HIV (17, 40). These studies demonstrated the phosphorylation of FLT to the respective MP and triphosphate and the incorporation into the DNA. Interestingly, pharmacokinetic data indicate that the compound accumulates mainly as MP and that the level of the triphosphate is $<$20% of the level of the MP (17). We found comparable DNA incorporation of [^{18}F]-FLT in pancreatic cancer cells, but not in short-time culture of primary tissue (27). However, because of the chemical modification of [^{18}F]-FLT, we propose a lower efficiency of incorporation of [^{18}F]-FLT into the DNA as compared with unmodified nucleosides. In this respect, it has to be noted that recent studies failed to prove substantial incorporation of [^{18}F]-FLT into the DNA (14, 20). These conflicting findings might relate to different experimental settings used.

In mice, we found a correlation of [^{18}F]-FLT uptake with the BrdUrd-labeling index in DoHH2 derived tumors. Furthermore, increased uptake of [^{18}F]-FLT was found in the spleen, which represents an organ with a high-proliferative activity in mice. The uptake in the tumor and the spleen increased over a period of 60 min. This time course, together with the metabolic stability, displays a major advantage of [^{18}F]-FLT as PET tracer compared with [^{11}C]thymidine (11, 12) and [^{18}F]fluoro-2′-deoxyuridine (13). The metabolic stability of [^{18}F]FLT is related at least in part to the lack of dephosphorylation through thymidine phosphorylase (14, 41). In sharp contrast, the uptake of [^{18}F]FLT in all other organs displayed a washout kinetic that reflected the presence of [^{18}F]FLT in the blood with slightly higher values in the kidney suggesting a renal excretion.

On the basis of these promising results, we performed a pilot study in patients with malignant lymphoma and compared [^{18}F]FLT with FDG-PET. FDG-PET displays a powerful tool for accurate staging and evaluation of residual masses of malignant lymphoma. Several studies indicate that FDG-PET is superior to anatomical imaging procedures in this respect (4–6). However, clinical questions such as low-grade lymphoma in transformation, mixed response to therapy, and prediction of relapse still pose diagnostic problems. First we confirmed the stability of [^{18}F]FLT in the serum of human patients *in vivo* with HPLC analysis. Furthermore, our HPLC analysis indicated that [^{18}F]-FLT is excreted both as paternal- and as glucuronide-conjugated compounds. However, the definitive identification of the urinary metabolite awaits suitable standards (20). Whole body PET scans with [^{18}F]FLT as tracer demonstrated increased accumulation in the bone marrow and in the liver. In contrast to our findings in mice, we did not observe substantial uptake in the spleen consistent with the lack of hematopoiesis in this organ in humans. However, considerable uptake of [^{18}F]FLT was found in the liver, which was consistent with the glucuronidation of the tracer in humans (20).

In comparison with FDG, we found that both tracers detected a similar number of lesions. Furthermore, we found a close correlation of the proliferation index with the SUV in 8 of 9 patients in our pilot study. These observations indicated that [^{18}F]FLT-PET represents both a novel tool for the diagnosis and staging of human malignant lymphoma and a noninvasive measurement of proliferation in these tumors. Nevertheless, [^{18}F]FLT-PET underestimated the proliferation in one patient with aggressive lymphoma with low cellularity and marked desmoplastic reaction. The unique biological properties of this kind of tumor offer a straight explanation for the low uptake of [^{18}F]FLT. However, this clearly indicates the probable limitations of this tracer to provide a measurement of proliferation. We suggest that a careful selection of patients in future studies will be essential in establishing the advantages and disadvantages of [^{18}F]FLT as a novel PET tracer. Furthermore, to answer clinical questions such as assessment of successful therapy, evaluation of living tumor cells in residual masses, and early prediction of relapse, these studies (for review see Refs. 20 and 16) need to reveal whether [^{18}F]FLT adds clinically important information to conventional FDG-PET.

REFERENCES

1. Goldberg, M. A., Lee, M. J., Fischman, A. J., Mueller, P. R., Alpert, N. M., and Thrall, J. H. Fluorodeoxyglucose PET of abdominal and pelvic neoplasms: potential role in oncologic imaging. Radiographics, *13:* 1047–1062, 1993.
2. Higashi, T., Tamaki, N., Honda, T., Torizuka, T., Kimura, T., Inokuma, T., Ohshio, G., Hosotani, R., Imamura, M., and Konishi, J. Expression of glucose transporters in human pancreatic tumors compared with increased FDG accumulation in PET study. J. Nucl. Med., *38:* 1337–1344, 1997.
3. Reske, S. N., Grillenberger, K. G., Glatting, G., Port, M., Hildebrandt, M., Gansauge, F., and Beger, H. G. Overexpression of glucose transporter 1 and increased FDG uptake in pancreatic carcinoma. J. Nucl. Med., *38:* 1344–1348, 1997.
4. Bangerter, M., Moog, F., Buchmann, I., Kotzerke, J., Griesshammer, M., Hafner, M., Elsner, K., Frickhofen, N., Reske, S. N., and Bergmann, L. Whole-body 2-[18F]-fluoro-2-deoxy-D-glucose positron emission tomography (FDG-PET) for accurate staging of Hodgkin's disease. Ann. Oncol., *9:* 1117–1122, 1998.
5. Carr, R., Barrington, S. F., Madan, B., O'Doherty, M. J., Saunders, C. A., van der Walt, J., and Timothy, A. R. Detection of lymphoma in bone marrow by whole-body positron emission tomography. Blood, *91:* 3340–3346, 1998.
6. Moog, F., Bangerter, M., Diederichs, C. G., Guhlmann, A., Kotzerke, J., Merkle, E., Kolokythas, O., Herrmann, F., and Reske, S. N. Lymphoma: role of whole-body 2-deoxy-2-[F-18]fluoro-D-glucose (FDG) PET in nodal staging. Radiology, *203:* 795–800, 1997.
7. Moog, F., Bangerter, M., Diederichs, C. G., Guhlmann, A., Merkle, E., Frickhofen, N., and Reske, S. N. Extranodal malignant lymphoma: detection with FDG PET versus CT. Radiology, *206:* 475–481, 1998.
8. Moog, F., Bangerter, M., Kotzerke, J., Guhlmann, A., Frickhofen, N., and Reske, S. N. 18-F-fluorodeoxyglucose-positron emission tomography as a new approach to detect lymphomatous bone marrow. J. Clin. Oncol., *16:* 603–609, 1998.
9. Jerusalem, G., Beguin, Y., Fassotte, M. F., Najjar, F., Paulus, P., Rigo, P., and Fillet, G. Whole-body positron emission tomography using 18F-fluorodeoxyglucose for posttreatment evaluation in Hodgkin's disease and non-Hodgkin's lymphoma has higher diagnostic and prognostic value than classical computed tomography scan imaging. Blood, *94:* 429–433, 1999.
10. Lapela, M., Leskinen, S., Minn, H. R., Lindholm, P., Klemi, P. J., Soderstrom, K. O., Bergman, J., Haaparanta, M., Ruotsalainen, U., Solin, O., *et al.* Increased glucose metabolism in untreated non-Hodgkin's lymphoma: a study with positron emission tomography and fluorine-18- fluorodeoxyglucose. Blood, *86:* 3522–3527, 1995.
11. Martiat, P., Ferrant, A., Labar, D., Cogneau, M., Bol, A., Michel, C., Michaux, J. L., and Sokal, G. *In vivo* measurement of carbon-11 thymidine uptake in non-Hodgkin's lymphoma using positron emission tomography. J. Nucl. Med., *29:* 1633–1637, 1988.
12. Mankoff, D. A., Shields, A. F., Link, J. M., Graham, M. M., Muzi, M., Peterson, L. M., Eary, J. F., and Krohn, K. A. Kinetic analysis of 2-[^{11}C]thymidine PET imaging studies: validation studies. J. Nucl. Med., *40:* 614–624, 1999.
13. Seitz, U., Wagner, M., Vogg, A. T., Glatting, G., Neumaier, B., Greten, F. R., Schmid, R. M., and Reske, S. N. *In vivo* evaluation of 5-[(18)F]fluoro-2′-deoxyuridine as tracer for positron emission tomography in a murine pancreatic cancer model. Cancer Res., *61:* 3853–3857, 2001.
14. Shields, A. F., Grierson, J. R., Dohmen, B. M., Machulla, H. J., Stayanoff, J. C., Lawhorn-Crews, J. M., Obradovich, J. E., Muzik, O., and Mangner, T. J. Imaging proliferation *in vivo* with [F-18]FLT and positron emission tomography. Nat. Med., *4:* 1334–1336, 1998.
15. Buck, A. K., Schirrmeister, H., Hetzel, M., Von Der Heide, M., Halter, G., Glatting, G., Mattfeldt, T., Liewald, F., Reske, S. N., and Neumaier, B. 3-deoxy-3-[(18)F]fluorothymidine-positron emission tomography for noninvasive assessment of proliferation in pulmonary nodules. Cancer Res., *62:* 3331–3334, 2002.
16. Rasey, J. S., Grierson, J. R., Wiens, L. W., Kolb, P. D., and Schwartz, J. L. Validation of FLT uptake as a measure of thymidine kinase-1 activity in A549 carcinoma cells. J. Nucl. Med., *43:* 1210–1217, 2002.
17. Kong, X. B., Zhu, Q. Y., Vidal, P. M., Watanabe, K. A., Polsky, B., Armstrong, D., Ostrander, M., Lang, S. A., Jr., Muchmore, E., and Chou, T. C. Comparisons of anti-human immunodeficiency virus activities, cellular transport, and plasma and intracellular pharmacokinetics of 3′-fluoro- 3′-deoxythymidine and 3′-azido-3′-deoxythymidine. Antimicrob. Agents Chemother., *36:* 808–818, 1992.
18. Belt, J. A., Marina, N. M., Phelps, D. A., and Crawford, C. R. Nucleoside transport in normal and neoplastic cells. Adv. Enzyme Regul., *33:* 235–252, 1993.
19. Mackey, J. R., Mani, R. S., Selner, M., Mowles, D., Young, J. D., Belt, J. A., Crawford, C. R., and Cass, C. E. Functional nucleoside transporters are required for gemcitabine influx and manifestation of toxicity in cancer cell lines. Cancer Res., *58:* 4349–4357, 1998.
20. Mier, W., Haberkorn, U., and Eisenhut, M. [18F]FLT; portrait of a proliferation marker. Eur. J. Nucl. Med. Mol. Imaging, *29:* 165–169, 2002.
21. Sherley, J. L., and Kelly, T. J. Regulation of human thymidine kinase during the cell cycle. J. Biol. Chem., *263:* 8350–8358, 1988.

22. Sakamoto, S., Ebuchi, M., and Iwama, T. Relative activities of thymidylate synthetase and thymidine kinase in human mammary tumours. Anticancer Res., *13:* 205–207, 1993.
23. Romain, S., Martin, P. M., Klijn, J. G., van Putten, W. L., Look, M. P., Guirou, O., and Foekens, J. A. DNA-synthesis enzyme activity: a biological tool useful for predicting anti-metabolic drug sensitivity in breast cancer? Int. J. Cancer, *74:* 156–161, 1997.
24. Kluin-Nelemans, H. C., Limpens, J., Meerabux, J., Beverstock, G. C., Jansen, J. H., de Jong, D., and Kluin, P. M. A new non-Hodgkin's B-cell line (DoHH2) with a chromosomal translocation t(14;18)(q32;q21). Leukemia, *5:* 221–224, 1991.
25. de Kroon, J. F., Kluin, P. M., Kluin-Nelemans, H. C., Willemze, R., and Falkenburg, J. H. Homing and antigenic characterization of a human non-Hodgkin's lymphoma B cell line in severe combined immunodeficient (SCID) mice, Leukemia. *8:* 1385–1391, 1994.
26. Cotter, F. E., Johnson, P., Hall, P., Pocock, C., al Mahdi, N., Cowell, J. K., and Morgan, G. Antisense oligonucleotides suppress B-cell lymphoma growth in a SCID-hu mouse model. Oncogene, *9:* 3049–3055, 1994.
27. Seitz, U., Wagner, M., Neumaier, B., Wawra, E., Glatting, G., Leder, G., Schmid, R. M., and Reske, S. N. Evaluation of pyrimidine metabolising enzymes and *in vitro* uptake of 3′- [(18)F]fluoro-3′-deoxythymidine ([(18)F]FLT) in pancreatic cancer cell lines. Eur. J. Nucl. Med. Mol. Imaging, *29:* 1174–1181, 2002.
28. Siegmund, H, and Pfleiderer, W. The synthesis of phospholipid conjugates of antivirally active nucleosides by the improved phosphoramidite methodology. Helv. Chim. Acta. 79*:* 426–438, 1996.H. P.
29. Machulla, H. J., Blocher, A., Kuntzsch, M., Piert, M., Wei, R., Grierson, J. R. Simplified Labeling Approach for Synthesizing 3′-Deoxy-3′-[18F]Fluorothymidine ([18F]FLT). J. Rad. Nucl. Chem., *243:* 843–846, 2000.
30. Richards, G. M. Modifications of the diphenylamine reaction giving increased sensitivity and simplicity in the estimation of DNA. Anal. Biochem., *57:* 369–376, 1974.
31. Voit, C., Mayer, T., Proebstle, T. M., Weber, L., Kron, M., Krupienski, M., Zeelen, U., Sterry, W., and Schoengen, A. Ultrasound-guided fine-needle aspiration cytology in the early detection of melanoma metastases. Cancer, *90:* 186–193, 2000.
32. Eriksson, S., Arner, E., Spasokoukotskaja, T., Wang, L., Karlsson, A., Brosjo, O., Gunven, P., Julusson, G., and Liliemark, J. Properties and levels of deoxynucleoside kinases in normal and tumor cells; implications for chemotherapy. Adv. Enzyme Regul., *34:* 13–25, 1994.
33. Clavo, A. C., Brown, R. S., and Wahl, R. L. Fluorodeoxyglucose uptake in human cancer cell lines is increased by hypoxia. J. Nucl. Med., *36:* 1625–1632, 1995.
34. Kubota, R., Kubota, K., Yamada, S., Tada, M., Ido, T., and Tamahashi, N. Microautoradiographic study for the differentiation of intratumoral macrophages, granulation tissues and cancer cells by the dynamics of fluorine-18-fluorodeoxyglucose uptake. J. Nucl. Med., *35:* 104–112, 1994.
35. Haberkorn, U., Ziegler, S. I., Oberdorfer, F., Trojan, H., Haag, D., Peschke, P., Berger, M. R., Altmann, A., and van Kaick, G. FDG uptake, tumor proliferation and expression of glycolysis associated genes in animal tumor models. Nucl. Med. Biol., *21:* 827–834, 1994.
36. Ito, M., and Conrad, S. E. Independent regulation of thymidine kinase mRNA and enzyme levels in serum-stimulated cells. J. Biol. Chem., *265:* 6954–6960, 1990.
37. Arner, E. S., and Eriksson, S. Mammalian deoxyribonucleoside kinases. Pharmacol. Ther., *67:* 155–186, 1995.
38. Kristensen, T., Jensen, H. K., and Munch-Petersen, B. Overexpression of human thymidine kinase mRNA without corresponding enzymatic activity in patients with chronic lymphatic leukemia. Leuk. Res., *18:* 861–866, 1994.
39. Plagemann, P. G. W., and Wohlhueter, R. M. Permeation of nucleosides, nucleic acid bases, and nucleotides in animal cells. *In:* F. Bronner and A. Kleinzeller (eds.), Current Topics in Membranes and Transport XIV, pp. 225–330. New York: Academic Press, 1980.
40. Sundseth, R., Joyner, S. S., Moore, J. T., Dornsife, R. E., and Dev, I. K. The anti-human immunodeficiency virus agent 3′-fluorothymidine induces DNA damage and apoptosis in human lymphoblastoid cells. Antimicrob. Agents Chemother. *40:* 331–335, 1996.
41. Balzarini, J., Baba, M., Pauwels, R., Herdewijn, P., and De Clerq, E. Anti-retrovirus activity of 3′-fluoro- and 3′-azido-substituted pyrimidine 2′,3′-dideoxynucleoside analogues. Biochem. Pharmacol., *37:* 2847–2856, 1988.